Supplementary Figures:

Supplementary Movie 1 (SM1)
Movie showing the action potential propagation in wild type linear heart tube at 24 hpf. Action potential propagation is slow and homogeneous.

Supplementary Movie 2 (SM2)
Movie showing the action potential propagation in wild type heart at 72 hpf, after looping is complete.

Supplementary Movie 3 (SM3)
Movie showing the action potential propagation in a heart from Wnt11 MO morphant embryo at 72 hpf.

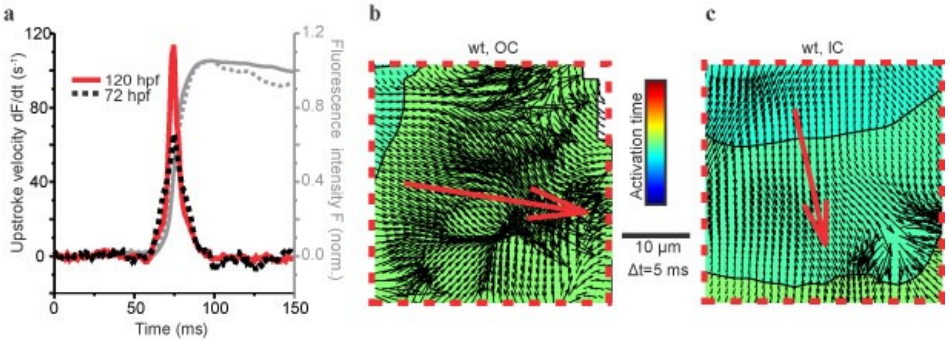

Supplementary Figure 1: Estimation of conduction velocity vector fields.
a, Upstrokes (grey) and derived upstroke velocities at 72hpf (black) and 120hpf (red) of action potentials from wild type hearts at these time points demonstrate the increase in upstroke velocities through development. These data confirm that the dynamic range of our optical mapping using the voltage sensitive dye di-8 ANEPPS is adequate for the measurement of changes in upstroke velocity during development.
b,**c**, Conduction velocity vector fields estimated from ROIs covering an area of about 35 x 35 µm of cardiac tissue within the OC (**b**) or the IC (**c**) of the same heart. The ROI is large enough to give a good estimate of conduction velocities, while remaining restricted to the inner or outer curvature of the developing ventricle. Errors resulting from variations in the positions of these ROIs were less than 10 % and smaller than the variations of these measurements between different hearts. All isochronal maps show ROIs in which conduction velocities were estimated from individual vectors (black arrows in **b**,**c**) that indicate the speed and direction of the propagating wave front at each point. The calculated average conduction velocities in each ROI are independent of the direction of wave front propagation and are the data depicted in each conduction velocity bar graph in the manuscript. We also calculated average conduction velocity vectors $\vec{w}$ (red arrow in **b**,**c**, scale factor 12.5). It is important to note that the magnitude of the average conduction velocity vector, $|\vec{w}|$, depends on the directions of the individual conduction velocity vectors $\vec{v}_i$ in the corresponding ROI, and thus is larger in ROIs where most vectors point in the same direction than in areas where many vectors point in different directions. The average velocity vectors (red arrows, scale factor 12.5) superimposed on each of the isochronal maps in the manuscript indicate a composite of the average direction and speed of electrical impulse propagation in the corresponding ROI. The colour code depicts the timing of electrical activation.

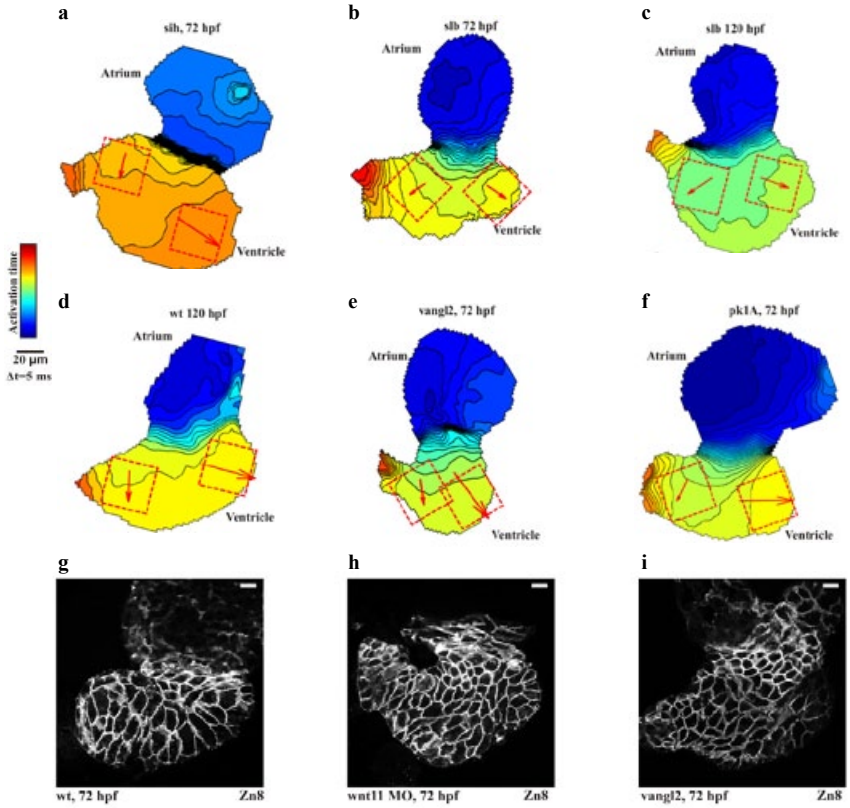

Supplementary Figure 2: Additional data confirming that loss of Wnt11 prevents myocardial electrical gradient.
a-f, Isochronal maps of hearts from silent heart at 72 hpf (**a**), silberblick (**b**) at 72 hpf, silberblick (**c**) and wild type (**d**) hearts at 120 hpf, vangl2 (**e**), Pk1A morphant (**f**) at 72 hpf. The colour code depicts the timing of electrical activation. The red squares indicate typical sample ROIs used for measurements in **Figure 2a, g, h, i, j**.
g-i, Z-projection of 1µm confocal sections of wild type (**g**), Wnt11morphant (**h**), and vangl2 (**i**) hearts isolated at 72hpf and stained with anti-Zn8 antibody to visualize the plasma membrane. Scale bars = 10 µm. The hearts were imaged on the same day and under identical conditions. The atrium is on the top, and the ventricle is below with outflow tract pointing to the left in all images.

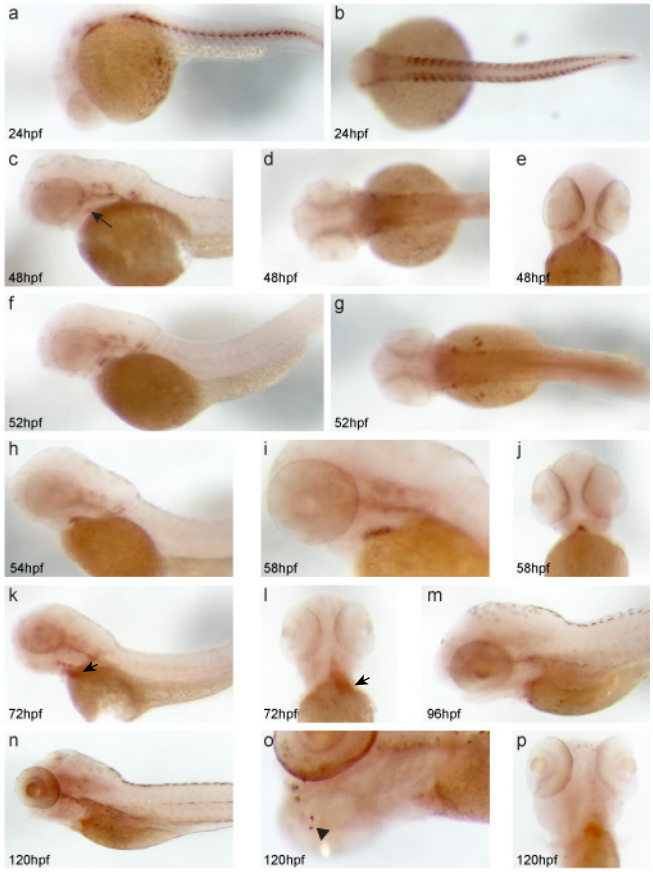

Supplementary Figure 3: Dynamic Wnt11 expression through embryonic and early larval stages.
Whole mount in situ hybridization of Wnt11 riboprobe at multiple embryonic stages (**a**-**j**). At 24hpf, Wnt11 is expressed in notochord, muscle pioneer cells and otic vesicle, lateral (**a**), dorsal (**b**) view. At 48hpf, expression localizes in otic vesicle and begins to be apparent in pharyngeal arches and outflow tract (arrow), lateral (**c**), dorsal (**d**), ventral (**e**) views. At 52hpf, expression intensifies in otic vesicle, pectoral fin buds, pharyngeal arches and outflow tract, lateral (**f**), dorsal (**g**) view. Expression in pharyngeal arches and outflow tract is further increased through 54hpf, lateral view (**h**) and is strongest at 58hpf, lateral (**i**), ventral (**j**) view. Wnt11 in situ hybridization at early larval stages (**k**-**p**). At 72hpf, Wnt11 expression is detected in the body of the cardiac ventricle, lateral (**k**), ventral (**l**) view, and persists through 96hpf, lateral view (**m**) and 120hpf, lateral (**n**, **o**), ventral (**p**) view. Arrow in **c** points to the outflow tract, in **k**, **l** to the cardiac ventricle and arrowhead in **o** points to the expression of Wnt11 in the nose. Anterior is on the left in lateral and dorsal views and on the top in ventral views.

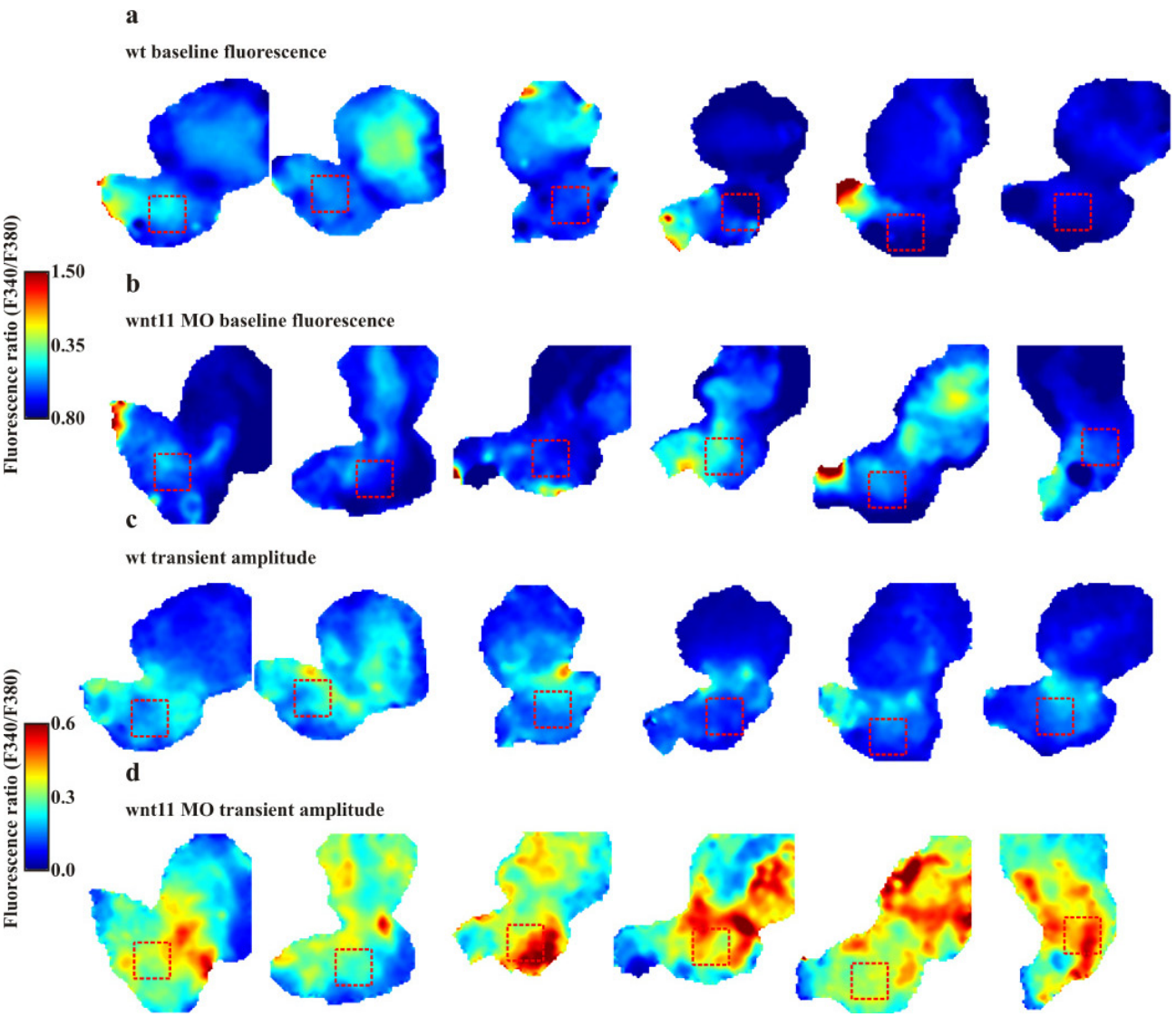

Supplementary Figure 4: Loss of Wnt11 causes heterogeneous increase in Ca^{2+} transient amplitudes.
a, **b**, Colour maps of baseline Ca^{2+} fluorescence in diastole from 6 individual wild type hearts (**a**) and 6 individual Wnt11 morphant hearts (**b**) demonstrating homogenous Ca^{2+} distribution. Colour code depicts Ca^{2+} diastolic concentrations in fluorescence ratio units (F340/F380).
c, **d**, Colour maps of Ca^{2+} transient amplitudes from the same individual hearts shown in panels **a**, **b**. While wild type Ca^{2+} transient amplitudes are homogenous (**c**), Wnt11 morphant Ca^{2+} transient amplitudes (**d**) exhibit significant heterogeneity across the heart. Colour code depicts Ca^{2+} diastolic concentrations in fluorescence ratio units (F340/F380). The red squares indicate ROIs used for measurements averaged in **Figure 3 d** in the main manuscript. The atrium is on the top, and the ventricle is below with outflow tract pointing to the left in all images. All measurements were obtained at 72hpf.

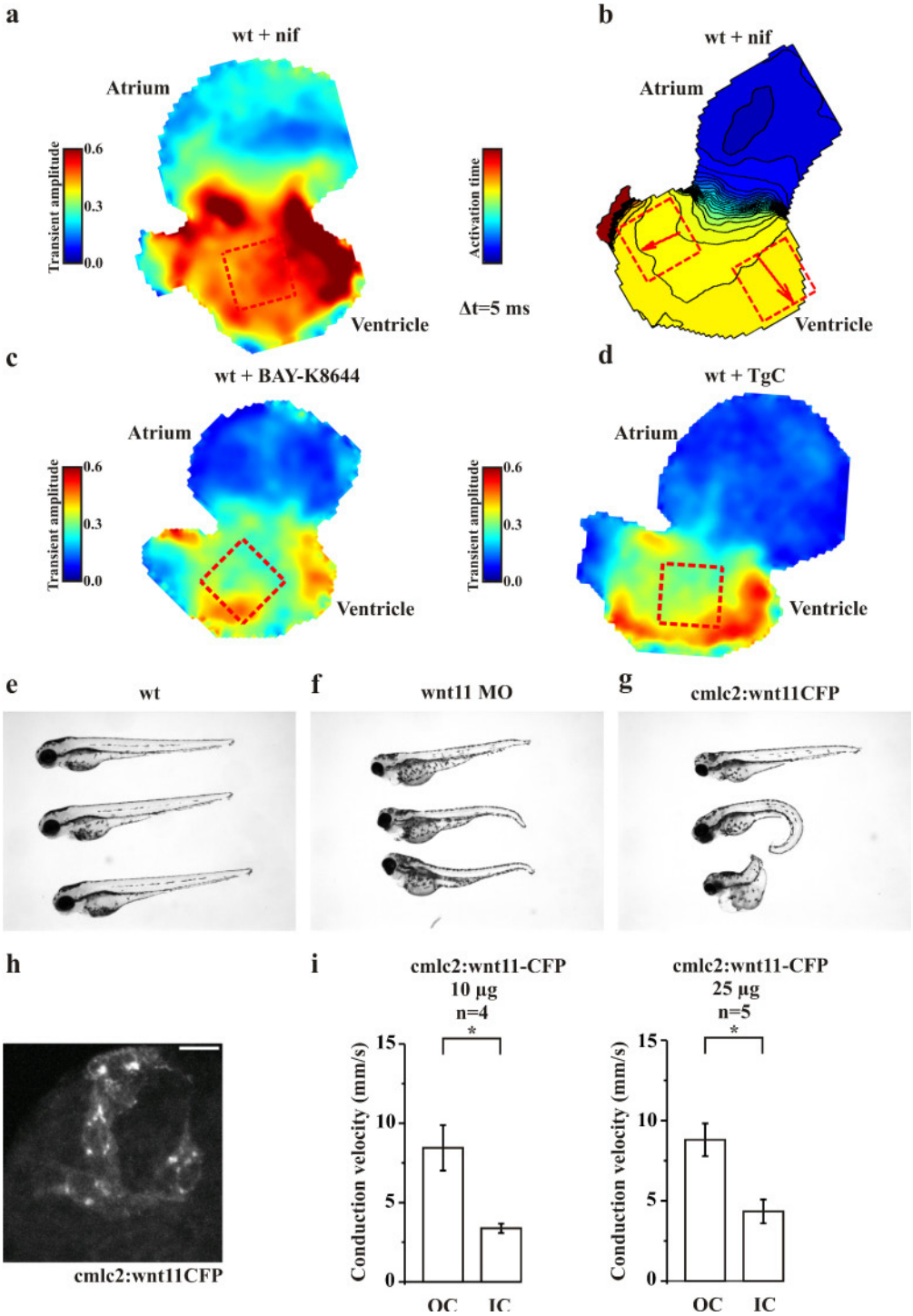

Supplementary Figure 5: Wnt11 patterns electrical coupling through effects on transmembrane Ca^{2+} conductance.

a, Colour map of Ca^{2+} transient amplitudes of hearts from nifedipine treated embryos. The colour code depicts diastolic Ca^{2+} concentrations in fluorescence ratio units (F340/F380). The red squares indicate ROIs used for measurements averaged in **Figure3d**.

b, Isochronal map of hearts from nifedipine treated embryos. The colour code depicts the timing of electrical activation. The red squares indicate ROIs used for measurements averaged in **Figure3i**.

c, **d**, Colour map of Ca^{2+} transient amplitudes of hearts from BayK-8644 (**c**) and Thapsigargin-Caffeine (**d**) treated embryos. The colour code depicts diastolic Ca^{2+} concentrations in fluorescence ratio units (F340/F380). The red squares indicate ROIs used for measurements averaged in **Figure4b**. The atrium is on the top, and the ventricle is below with outflow tract pointing to the left in all images.

e-**g**, Bright field image of wild type (**e**), Wnt11 morphant (**f**) and cmlc2::Wnt11:CFP (**g**) injected embryos. Both Wnt11 morphant embryos and cmlc2::Wnt11:CFP injected embryos show varying degrees of cyclopia and shortened body axis. In addition both exhibit defects in heart morphogenesis and looping.

h, Z-projection of 2µm confocal sections of heart isolated from cmlc2::Wnt11:CFP injected embryos. The construct is expressed in a mosaic manner in a few cardiomyocytes and CFP fluorescence localizes to perinuclear puncta. Scale bar = 10 µm.

i, Comparison of mean estimated conduction velocities of hearts from embryos injected with different doses (10 µg/µl or 25 µg/µl) of cmlc2::Wnt11:CFP DNA. While the morphological phenotypes are dose-dependent, the electrical gradient does not appear to be. Student's t-test, *p<0.05. All experiments were done at 72 hpf.

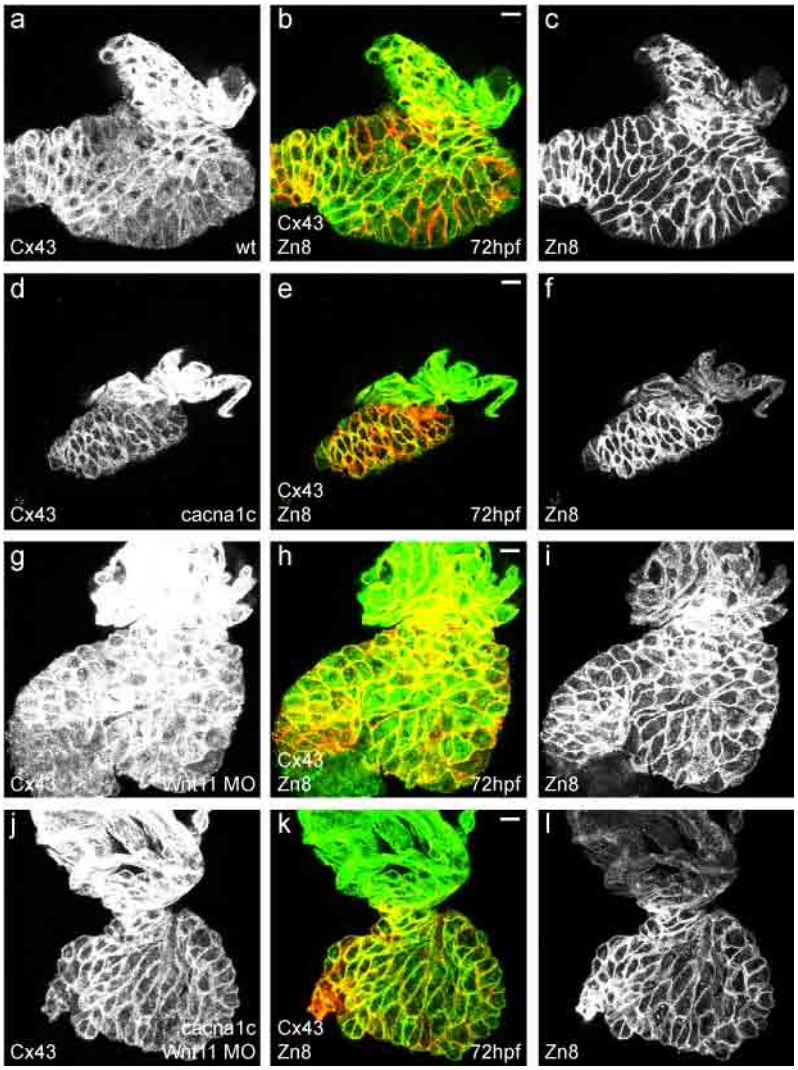

Supplementary Figure 6: Cx43 upregulation in the loss of Wnt11 is LTCC dependent.
Isolated hearts stained with anti-Cx43 (**a**, **d**, **g**, **j** and green in **b**, **e**, **h**, **k**) to label gap junctions and anti-Zn8 to visualize the plasma membrane (**c**, **f**, **i**, **l** and red in **b**, **e**, **h**, **k**). In wild type hearts (**a**-**c**) and in the LTCC mutant, *cacna1c* (**d**-**f**) Cx43 localizes to the plasma membrane and the cytoplasm. The cytoplasmic pool of Cx43 in *cacna1c* is slightly decreased. Cx43 is markedly upregulated in Wnt11 morphant hearts (**g**-**i**), both at the plasma membrane and in the cytoplasm (**g**, green in **h**), while Zn8 levels remain unchanged (**i**, red in **h**). The Cx43 localization and abundance (**i**, green in **k**) in *cacna1c* mutants with reduced Wnt11 levels are comparable to that observed in wild type hearts. Scale bar = 10 μm; all confocal images are 2μm Z-projections; the atrium is on the top and the ventricle is below with outflow tract pointing to the left in all images. All images were taken on the same day with the same laser and gain settings.

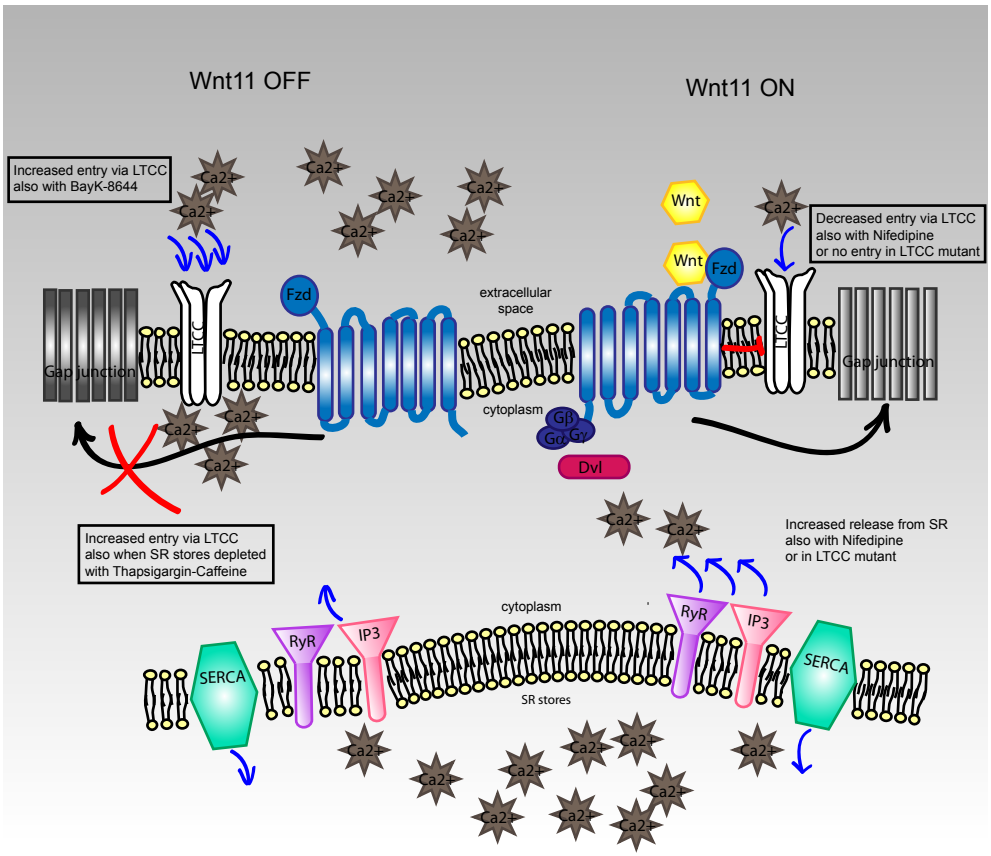

Supplementary Figure 7: Schematic of Wnt11 signaling operating through LTCC in the remodeling of cardiac electrical coupling.
The absence of Wnt11 results in a failure to decrease Ca^{2+} conductance specifically through the LTCC. The failure of this negative regulation of the LTCC leads to impaired and mispatterned electrical coupling within the developing heart. Similarly, applying the LTCC agonist BayK-8644 increases Ca^{2+} entry via the LTCC and abolishes physiologic formation of the myocardial electrical gradient. Depleting SR stores using Thapsigargin (a SERCA inhibitor) and Caffeine (a RyR agonist) also leads to increased LTCC conductance and prevents the remodeling of electrical coupling. In the presence of Wnt11 signal, LTCC conductance is attenuated and this results in active remodeling of electrical coupling and formation of an electrical gradient. Wnt11 signaling also results in increased Ca^{2+} release from SR stores, but this Ca^{2+} domain does not affect remodeling of electrical coupling. Additionally, enhanced Ca^{2+} release from SR stores occurs in LTCC mutants (*cacna1c*) or can be achieved using the LTCC antagonist, nifedipine. However, this source of Ca^{2+} does not affect electrical remodeling which continues unperturbed.